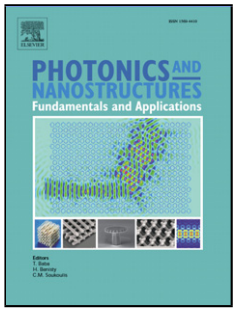

Title: Subwavelength gratings for polarization conversion and focusing of laser light

Authors: Sergey S. Stafeev, Victor V. Kotlyar, Anton G. Nalimov, Maria V. Kotlyar, Liam O'Faolain

PII: S1569-4410(17)30153-0
DOI: http://dx.doi.org/10.1016/j.photonics.2017.09.001
Reference: PNFA 607

To appear in: *Photonics and Nanostructures – Fundamentals and Applications*

Received date: 23-5-2017
Revised date: 11-9-2017
Accepted date: 13-9-2017

Please cite this article as: Sergey S.Stafeev, Victor V.Kotlyar, Anton G.Nalimov, Maria V.Kotlyar, Liam O'Faolain, Subwavelength gratings for polarization conversion and focusing of laser light, Photonics and Nanostructures - Fundamentals and Applicationshttp://dx.doi.org/10.1016/j.photonics.2017.09.001

Subwavelength gratings
for polarization conversion and focusing of laser light

Sergey S. Stafeev[1,2,*], Victor V. Kotlyar[1,2], Anton G. Nalimov[1,2], Maria V. Kotlyar[2], Liam O'Faolain[3]

[1]*Image Processing Systems Institute—Branch of the Federal Scientific Research Centre "Crystallography and Photonics" of the Russian Academy of Sciences, 151 Molodogvardeyskaya St., Samara 443001, Russia*
[2]*Samara National Research University, 34 Moskovskoye Shosse, Samara 443086, Russia*
[3]*Tyndall National Institute, Lee Maltings Complex, Dyke Parade, Cork, Ireland*

[*]*sergey.stafeev@gmail.com*

Highlights:

- we have analyzed subwavelength gratings to control the polarization of incident light
- the subwavelength gratings operating as wave-plate have been discussed
- a simple approach to designing metasurface components has been proposed

Abstract

We review thin micro-optics components with nanostructured microreliefs intended to control the polarization and phase of laser light. These components include transmission and reflection subwavelength diffraction gratings characterized by spatially -varying groove directions and fill factors, with the microrelief period and depth remaining approximately unchanged. In the visible spectrum, the microrelief features may vary in size from dozens to hundreds of nanometers. Segmented diffractive micropolarizers for linear to radial/azimuthal polarization conversion and subwavelength microlenses for tightly focusing the laser light are discussed in detail. Examples of particular micropolarizers and microlenses fabricated in amorphous silicon films are also given.

Keywords: subwavelength grating, metasurface, Pancharatnam–Berry phase, radially polarized light, azimuthally polarized light, metalens.

1. Introduction

Diffractive optical elements intended to modify the amplitude and phase of the transmitted/reflected light have been known in optics for quite some time [1]. However, it is only comparatively recently that researchers have taken an interest in studying elements capable of converting the polarization of light. Well-suited for this purpose are diffractive gratings with space variant grooves and subwavelength period, which are called subwavelength gratings [2]. In this case, there is only a zero diffraction order. The polarization control is implemented as follows. The local direction of grooves defines a chosen direction relative to which the polarization vector of the incident light can be decomposed into the TE- and TM- components, with these being, respectively, directed along and across the grooves. As light propagates

through a transparent diffraction grating, due to different effective refractive indices [3] the TE- and TM-waves acquire different phase shifts, making the output polarization vector rotate by some angle. If the phase shift equals a quarter of wavelength, the grating operates as a quarter-wave plate, performing the linear to circular polarization conversion [4], [5]. With a half-wavelength phase shift between the TE- and TM-components, the grating operates as a half-wave plate [6], [7]. In the visible spectrum, obtaining a half-wave phase shift in a low-refractive-index transparent material requires the fabrication of a microrelief whose depth is of the order of wavelength. For the subwavelength gratings, creating nano-sized microrelief features is a challenge [6]. Because of this, the gratings are either fabricated from high-index materials, resulting in the deteriorated grating transmittance, or utilized in reflection, rather than transmission, mode. To control the polarization of the incident light, one needs to calculate the period, fill factor, microrelief depth, and direction of the grating grooves at each point of the surface. For this purpose, the rigorous solution of vector Maxwell's equations is used.

Recently, optical elements capable of simultaneously controlling the polarization and phase of light have also been reported and are known as metasurface photonic components [8]. When used for focusing light they are called metalenses. As a rule, the metalens is calculated based on the Pancharatnam-Berry phase [9], [10] and can only operate with circularly polarized incident light. This is a drawback, as the circular polarization is generated using an extra element - a quarter-wave plate. However, the phase of light can be controlled in a different way. For instance, when designing a metalens, radii of zones of a Fresnel lens for a required focal length and required incident wavelength are calculated. Each metalens zone is then filled with binary diffraction gratings, each rotating the electric vector of the normally incident linearly polarized laser light by a pre-defined angle in such a manner that the output light is radially polarized [11]. The period, microrelief depth, and fill factor are selected in an optimal way via numerical modeling and on the assumption that the amplitude of light passing through each individual grating is approximately the same. The half-wavelength phase shift between adjacent metalens zones is implemented by two boundary-adjacent local gratings that are assumed to rotate the polarization vector by angles whose difference equals π.

In this review, we discuss space-variant subwavelength diffraction gratings intended to convert the polarization of light and metalenses. Subwavelength gratings in transmission and reflection modes that operate as analogs of quarter- and half-wave plates are discussed in detail. The use of such gratings for the implementation of linear to radial and azimuthal polarization conversion is described. In the final section, we give examples of metalenses for tightly focusing the laser light, which consist of subwavelength grating arrays.

2. Use of subwavelength gratings for light polarization conversion

The simplest way to perform the polarization conversion is through the use of subwavelength gratings. Such gratings have different refractive indices of the TE- and TM-components of the wave [3]:

$$n_{eff}^{TE} = \sqrt{d n_r^2 + (1-d) n_m^2} \tag{1}$$

$$n_{eff}^{TM} = \frac{1}{\sqrt{\left(\frac{d}{n_r^2} + \frac{1-d}{n_m^2} \right)}} \tag{2}$$

where d is the fill factor of the grating (the ratio of the step width to the grating period), n_r is the refractive index of the step material, and n_m is the refractive index of the environment.

Reference [2] was the first to demonstrate that subwavelength gratings are suitable for polarization conversion. Owing to a phase shift between the TE- and TM-waves transmitted through a subwavelength microrelief, the latter can be used as analogs of half- and quarter-wave

plates, and, consequently, convert the polarization of the incident light. Being easier to fabricate, micropolarizers based on the quarter-wave plates were the first to be implemented. The first experimental demonstration of light polarization conversion using subwavelength gratings analogous to the quarter-wave plates was reported in Refs. [4], [5], in which a circularly polarized beam of wavelength 10.6 μm was converted into an azimuthally polarized beam.

Some articles discussed here describe the use of subwavelength gratings for generating cylindrical vector beams. Such beams are characterized by radially symmetric polarization [12]. The radially polarized beams have found use for sharply focusing the laser light [13] and optical micromanipulation [14]. Note that azimuthally polarized beams are also utilized for sharply focusing the laser beams [15]. Moreover, when sharply focusing light, azimuthally polarized beams are preferable to radially polarized beams, because a subwavelength focal spot from the radially polarized beam is mainly composed of longitudinally polarized components - with almost no light coming from the focal spot along the axis to the observer - while a focal spot from an azimuthally polarized beam is mainly composed of transverse components, seen by the observer on the axis. For these reasons, the transversely polarized focal spots have been widely used in areas such as optical coherent tomography [16], optical data storage [17], and for detecting individual molecules [18].

In Ref. [19], a concentric metallic grating was utilized to convert the circularly polarized laser light at 633 nm into radially polarized light. The metallic grating was fabricated by coating a fused-silica substrate (n = 1.457) with a 200-nm aluminum layer, which was then coated with a 40-nm SiO_2 layer. Ellipsometric measurements showed the refractive index of Al to be n = 1.9907+8.518i (i.e. different from the reference value of n = 1.373+7.618i). The (axicon) grating composed of concentric rings with period 200 nm and fill factor 0.4 was defined using e-beam lithography in a resist layer, before being transferred into the SiO_2 layer using fluorine-based reactive ion etching and into the Al layer using chlorine-based reactive ion etching. However, the resulting beam [19] cannot in a strict sense be called radially polarized as it has identical phases at diametrically opposed points, whilst the said points of a "properly" radially polarized beam should be out of phase. To remedy the situation, a combined element has been proposed [20], [21] composed of a concentric metallic grating with 200-nm period and a "forked" hologram with 1.2 μm period. The element was fabricated in a 150-nm gold film coated on a glass substrate and experimentally tested at wavelengths 633 nm and 850 nm. A technique suitable for large-scale production of the quarter-wave plates based on subwavelength gratings has been described [22] – gratings with 360-nm period and the aspect ratio of 5.2 for the conversion of 633-nm light were fabricated using UV-moulding. Subwavelength gratings to convert linearly polarized beams into circularly polarized beams at 488 nm, 532 nm, and 632.8 nm have also been reported [23]. Such gratings may find uses in designing 3D displays [24].

Practical implementation of a half-wave plate requires a higher aspect ratio of individual grating elements, making it harder to fabricate. The grating microrelief features need to be twice as high as those of a quarter-wave plate. The operation of the subwavelength grating as an analog of a half-wave plate was first demonstrated in Ref. [25]. In fact, three grating micropolarizers different in design were studied. All three micropolarizers were fabricated in GaAs and intended to operate at 10.6 μm (CO_2 laser). It is also worth noting that the gratings fabricated in [25] had a varying period ranging from d_{min} = 2 μm to d_{max} = 3.05 μm. A subwavelength grating functionally analogous to a half-wave plate operating in the near infrared spectrum was synthesized in [6]. The grating converted a linearly polarized beam at 1064 nm into a radially polarized beam. The grating's template was written in a ZEP 520A resist using e-beam lithography, prior to being transferred into a GaAs substrate (refractive index n=3.478) using ion etching. Unlike Ref. [25] the grating had a constant period of 240 nm. An interferometer based on the grating [6] was proposed in Ref. [26]. In [6], the grating micropolarizer was fabricated in a high refractive index substrate. In a different approach proposed in Ref. [27], the grating was

fabricated in a low-index substrate. Such an approach boasts a number of advantages, such as lower aspect ratio of the microrelief elements and a 100% transmittance for one of the modes.

Reference [28] reported the fabrication of a micropolarizer using a silicon-on-insulator technique, to convert a linearly polarized beam into radially/azimuthally polarized light for wavelengths ranging from 1030 nm to 1064 nm. The micropolarizer made of hydrogenated amorphous silicon (refractive index n = 3.4) was fabricated in a low-index substrate (fused silica n = 1.45). In Refs. [29], [30] similar techniques were employed to fabricate a 4-sector micropolarizer in transmission with a phase shift. The micropolarizer in Fig. 1 was fabricated by electron beam lithography. The surface of a 130-nm thick amorphous silicon (a-Si) found on a transparent pyrex 7740 substrate (refractive index is 1.47, http://www.valleydesign.com/pyrex.htm) was coated with a 320-nm thick PMMA resist, which was then baked at 180C. To prevent charging the sample surface was coated with a 15-nm thick golden layer. The four-sector grating-polarizer's pattern was created on the resist surface by a 30-kV electron beam. The sample was developed in a 3:7 water solution of isopropanol and the gold layer was removed. The transfer of the grating-polarizer's template from the resist to the aSi was carried out via reactive ion etching in a gas mixture of CHF3 and SF6 using a recipe optimized for photonic crystal fabrication similar to that used in [31]. The resist thickness was chosen so as to enable the protection of the pattern during the etching of the 130-nm aSi. The aspect ratio of etch rates of the material and the mask was found to be 1:2.5.

The four-sector micropolarizer in transmission converts an incident laser beam of wavelength λ = 633 nm into an azimuthally polarized beam with a phase shift such that at the diametrically opposite points of the beam cross-section the polarization is the same. In Ref. [29], a laser beam transmitted through a micropolarizer was focused with a quartz binary zone plate (ZP) (Fig.2a) with wavelength focus into a subwavelength focal spot. Measurements with a near-field scanning optical microscope (NSOM) [7] have shown a focal spot to be formed at a distance of 200-250 nm from the ZP surface, with the spot size being FWHM = 0.46λ and FWHM = 0.57λ (Fig. 2b).

The conversion of light polarization by means of subwavelength gratings was also discussed in Refs. [32]–[34]. A grating of 400-nm period in a fused silica substrate coated with a TiO_2 layer and operating as a half-wave plate was reported in Ref. [32]. The grating was intended to operate at 628 nm and found to have a 90% transmittance. A subwavelength grating of 410-nm period in slanted photonic structures was reported in Ref. [34]. The grating was fabricated by coating a fused silica substrate with a 640-nm thick TiO_2 layer prior to applying atop a Cr grating, which was then used as a mask. During the ion etching process, the specimen was fixed so as to ensure that the etched groove had a slant of about 30º to the surface normal. After etching, the chrome remainders were removed. Despite the over-etched microrelief, the grating showed high transmittance of 95.5%, also producing a 177-degree phase shift between the TE- and TM-waves (i.e. very close to a half-wave plate).

An achromatic IR wave plate fabricated by imprinting and producing a 30º phase shift in transmission mode at wavelengths 8.5 μm – 10.5 μm was discussed in Ref. [35]. The grating had a 3-μm period, a 1.63-μm microrelief depth, and a fill factor of 0.07. At the first stage, a mold with a 3-μm period and a fill factor of 0.5 was fabricated. A glassy carbon substrate was coated with a layer of WSi and a photoresist, with the latter being then exposed to a 442-nm He-Cd laser. After removing the exposed photoresist, the WSi layer was exposed to the reactive ion etching in SF_6, with the glassy carbon being etched in O_2. The exposure time was selected so as to attain a 1.94-μm microrelief depth. Using the mold, the grating under study was imprinted into the chalcogenide glass, which has n=2.7 in the wavelength range of interest and sulphur as its major component (a Sb-Ge-Sn-S system). The temperature, pressure, and time of imprinting were, respectively, 253C, 3.8 Pa, and 90 s. In another work by the same authors [36], fabrication of a micropolarizer for wavelengths 5 μm - 9 μm was reported. The grating polarizer had a 260-nm microrelief depth, a 500-nm groove width, and a 290-nm rod width. The grating reported in

Ref. [37] was also fabricated by imprinting, but it was intended for visible light. The grating with a 300-nm period was fabricated in a Bi_2O_3-GeO_2-B_2O_3 glass. At the wavelength of 400 nm the grating was able to produce a phase shift of 0.23λ. An effective technique for designing wave plates was proposed in [38].

3. Reflecting gratings

When fabricating a half-wave plate, the high aspect ratio requirement can be obviated via using a reflecting, rather than transmission, grating. In this case, the microrelief height is halved. A reflecting micropolarizer to perform linear-to-radial polarization conversion of light was described in [7], [39]. The micropolarizer was designed as a four-sector subwavelength grating, with the angle between the grooves and the incident polarization vector being different in each sector. In the sectors, the polarization vector was, respectively, rotated by the angles of 45, -45, 135, or -135º (Fig. 3).

Figure 4 depicts numerically simulated plots when linearly polarized light is reflected at a subwavelength grating whose parameters are described in Fig. 3. The simulation was based on solving Maxwell's equations using a FDTD-method in the FullWAVE (RSoft) software.

Figure 4 depicts the reflected light intensity $|E_2|^2$ and the polarization angle θ versus the angle α. From Fig. 4b the intensity is seen to vary in a wide range with varying angle of the grating's groove tilt α. Hence, we can infer that to be able to form a reflected field with a maximally uniform intensity pattern it will suffice to use just four sectors with differently oriented grating grooves. This enables us to avoid using regions characterized by a maximum reflected intensity (amounting to, or more than 0.7 relative units in Fig 4b). With a four-sector polarizer, the difference between the angles θ in each adjacent sector needs to be 90°. Taking this and Fig. 4a,b into account, we infer that the angles α = ±40° and ±70° are most suitable, as in this case the difference between the reflected intensities from the different sectors is minimal. Then, the respective angles of the polarization rotation are given by -135°, -45°, 45°, and 135°. In the course of modeling, the period of the diffraction gratings in all four sectors in Fig. 4 was assumed to be 0.4 μm for all angles α. Then, to obtain a maximally uniform intensity of the light reflected at four micropolarizer sectors with the angles α = ±40° and ±70° the grating periods were optimized. Optimal periods were found to be different, being equal to 0.4 μm for the sectors with the angles α=±40° and to 0.46 μm for the sectors with the angles α=±70°. Prior to optimizing the grating periods, the ratio of the reflected intensity to the incident one for α=±40° and α=±70° was, respectively, 58% and 43.3% (Fig. 4b). Following the optimization, the reflectance for α = ±70° reached 51% [40], [41].

The reflecting micropolarizer (Fig.5a) for linear-to-radial polarization conversion [7], [39] was fabricated using e-beam lithography. A glass substrate was coated with a 160-180-nm gold film, which was then coated with a resist layer. A template of the four-sector grating polarizer was then projected onto the resist using a 30-kV electron beam. By way of development, the specimen was then etched in xylene to remove the resist areas exposed to the electron beam. Next, the grating template was transferred into the gold layer by ion milling of the gold film from resist-free areas. Finally, resist remnants were removed using oxygen plasma, with the resulting micropolarizer template being 'engraved' in gold. The reactive ion etching time was optimized so as to achieve an etch depth of about 110 nm. A micropolarizer fabricated using the same procedure but intended to obtain an azimuthally polarized beam (Fig. 5b) was reported in Refs. [40], [41].

Figure 6a shows an image of the four-sector micropolarizer of Fig. 5a obtained using an output polarizer with its axis directed vertically, considering that the incident light is linearly polarized in the horizontal plane. In this case, all four sectors of the micropolarizer turn out to be bright (Fig. 5a). Note that two right sectors of the micropolarizer have a higher (on 10%) reflectance when compared with the two left ones. Although it is possible to achieve equal

reflection coefficients in the four sectors but the price to be paid is different periods and fill factors of the gratings in each sector. Figure 6b shows a micropolarizer image obtained when the axis of the polarizer placed in reflected light is rotated by 45º about the horizontal axis. Figure 6c shows the same pattern but with the output polarizer axis rotated by -45º about the horizontal axis. In this case, two of four micropolarizer's sectors found on the diagonals are observed as bright.

*a)*Figure 7 depicts images of the micropolarizer in Fig. 5*b* with a polarizer P placed in front of the CCD-camera and making angles 0° (a), -45° (c), and 45° (d) with the incident light polarization axis. From Fig. 7, the light reflected at the micropolarizer (Fig. 5b) is seen to be azimuthally polarized. The reflected beam was then directed to the binary microlens of Fig. 2a, producing a sharp focus. Figure 8 illustrates a SNOM-aided intensity pattern, with the minimal and maximal size of the focal spot measuring $FWHM_{min} = (0.35\pm0.02)\lambda$ and $FWHM_{max} = (0.38\pm0.02)\lambda$.

A reflective wave plate of period 400 nm, fill factor 0.5, and microrelief depth 280 nm was reported in Refs. [42], [43]. Comparison with a transmission grating with the same period and fill factor, but a twice deeper microrelief (450 nm) was made. As distinct from Refs. [39], [41] the microrelief of the gratings in Refs. [42], [43] was fabricated in a photoresist layer, with the operation in reflection achieved via using a silicon substrate, unlike a glass substrate of the transmission grating. Both gratings were numerically and experimentally shown to produce the same phase retardation.

4. Terahertz grating micropolarizers

In the bulk of works concerned with the exploitation of the subwavelength gratings as wave plates, a relatively large proportion of papers discuss the terahertz waveband. For instance, in Refs. [44], [45], the quarter-wave plates for frequencies 2.6 THz, 3.2 THz, and 3.8 THz were implemented as gratings with a 60-μm period and microrelief depths of 330 μm, 280 μm and 230 μm, respectively. A grating with period 20 μm, fill factor 0.5, and microrelief depths of 46 μm and 30 μm for respective frequencies 1.5 THz and 2.8 THz was considered in Ref. [46]. The grating fabricated of silicon had an antireflection coating SU8, enabling a 21% increase in the transmittance. A quarter-wave plate implemented in [47] operated at 0.51 THz, having a period of 30 μm and a microrelief depth of 156 μm. In [48], a grating of period 10 μm and microrelief depth 6 μm was utilized as a quarter-wave range plate for a 10 THz frequency. A quarter-wave plate for low-frequency terahertz waveband in the 200 - 330 GHz range was discussed in Ref. [49]. An achromatic quarter-wave plate operating at 0.47 - 0.8 THz was designed in [50]. In the experiment, fabrication errors showed to result in phase retardation errors of 3% when illuminating the plate with a 0.5-THz wave. A reflective achromatic quarter-wave plate for a waveband of 1.8 - 2.8 THz was studied in [51].

5. Subwavelength gratings as absorption-based polarizers

In the previous sections, we discussed the use of the subwavelength gratings as wave plates that converted the incident light polarization based on the difference between the effective refractive indices of the grating for TE- and TM-waves. However, this is not the only way the subwavelength gratings can perform the polarization conversion. It has been demonstrated [52] that in the subwavelength grating the absorption of a TM-wave is higher than that of a TE-wave. Such an effect can be employed to design analogs of "classical" polarizers.

Subwavelength micropolarizers operating in the visible spectrum were used for polarization imaging in [53]. An array composed of gratings with differently oriented grooves (0, 45º, 90º, and 135º) was nano-fabricated in an Al layer coated on a glass substrate by e-beam lithography and ion etching. The gratings had a rectangular groove profile with period 140 nm, fill factor 0.5, and microrelief depth 100 nm. An individual grating was 7.4×7.4 μm in size,

which is the same as the CCD cell size. After fabrication, the grating array was aligned with the CCD and utilized for real-time polarization imaging.

6. Subwavelength grating-based metalenses

In recent years, optical researchers have taken interest in studying planar binary microoptics components of subwavelength thickness composed of nanoscale arrays (rods, slits, stripes, gratings) made of metal or semiconductor, which are simultaneously capable of manipulating the polarization, amplitude, and phase of the incident light. Such photonic microcomponents are called metasurface components and reviewed in Ref. [8]. The metasurfaces can be utilized to generate optical vortices [54]; as broad-band near-IR sawtooth gratings capable of reflecting 80% of light within a desired angle [55]; to focus light into a doughnut intensity pattern [56] or a transverse line [57]. Of particular interest are ultrathin microlenses based on metasurfaces [58]–[63]. Note that while lenses proposed in Refs. [58]–[63] were implemented in the infrared spectrum, the only visible-spectrum lens operating at 550 nm was described in [63]. Metalenses based on metallic nanoarrays [58], [61], [62] showed a lower efficiency compared to those based on amorphous silicon [59], [60], [63]. The best characteristics have been demonstrated by a metalens composed of a silicon nano-rod array of diameter 200 nm and height ~1 μm [59]. The lens was shown to produce the minimal focal spot of diameter 0.57λ with an efficiency of about 40% for a linearly polarized incident beam. On the negative side is the high aspect ratio (5:1) of the lens [59], necessary for high-quality fabrication of the silicon rods. A binary microlens with a 100-μm focus and numerical aperture NA=0.43 for wavelength 550 nm was fabricated in Ref. [63]. The incident clockwise circularly polarized light was converted into an anticlockwise circularly polarized beam, before being focused into a 670-nm focal spot. The lens in question [63] was designed using a Pancharatnam-Berry phase and can operate only at the circularly polarized incident light, which is a drawback, as one needs to use an extra quarter-wave component to generate the circular polarization. Low NA is another drawback of the lens in [63]. A different approach to designing ultra-thin binary metalenses to focus linearly polarized laser light into a subwavelength circular focal spot beyond the diffraction limit was proposed in Ref. [64]. In this method, by arranging subwavelength binary diffraction gratings (four were shown to suffice) in each annular zone of a binary Fresnel zone plate, a linearly polarized incident beam was converted into a radially polarized beam. Based on this method, an ultra-thin metalens was designed and fabricated in an amorphous silicon film of diameter 30 μm and focal length equal to the incident wavelength of 633 nm, characterized by a subwavelength structure with a 220-nm period and 110-nm relief depth. Such a lens was shown to simultaneously control the polarization and phase of the incident light, converting linear polarization into the radial one and producing a sharp focus. The metalens was fabricated using e-beam lithography and ion etching.

The stages in designing and modeling the metalens from [65] are briefly described below. It has been known [64], [66] that when a linearly polarized laser beam is sharply focused using microoptics components (a binary axicon [64] or a binary zone plate [66]), the resulting subwavelength focal spot is elliptical. For instance, a glass binary ZP (n=1.5) of focus f=200 nm smaller than incident wavelength λ=532 nm and microrelief depth h=0.9 μm illuminated by a linearly polarized Gaussian laser beam of waist radius w=4λ produces a dumbbell-shaped elliptical focal spot elongated along the polarization axis at distance z=200 nm behind the ZP. Using an FDTD method implemented in the FullWAVE software, such a focal spot was found to measure at the full-width at half-maximum $FWHM_x$=0.85λ and $FWHM_y$=0.37λ (the ellipticity of 2.3:1) [65]. It is also known that by transforming the linearly polarized beam into the radially polarized one, a circular subwavelength focal spot can be obtained [13]. By way of illustration, a four-sector micropolarizer composed of subwavelength gratings was designed and fabricated in a gold film in [39], converting the incident linearly polarized laser light into the radially polarized light. It was shown that four sectors would suffice to generate a near radially polarized field [13], [39], which was then used for obtaining a subwavelength focal spot [7], [39]. A four-sector

micropolarizer in transmission mode was fabricated in an amorphous silicon film applied on a transparent substrate in [30]. The subwavelength grating had a period of T=230 nm and a microrelief depth of h=130 nm (λ=633 nm), with the refractive index of silicon chosen to equal n=3.87-i0.016. However, when focusing light using two separate elements (a reflective/transmission polarization converter and a zone plate), the optical setup needs to be precisely aligned, with the and extra energy being lost due to reflection at additional surfaces. This poses a problem of designing a microoptics component simultaneously capable of the polarization conversion of and sharply focusing the laser light. Such a subwavelength binary optical element can be designed by combining two optical elements discussed above. Shown in Fig. 9 is a metalens binary microrelief that combines the properties of a micropolarizer and a high-NA zone plate.

Parameters of the metalens in Fig. 9 are as follows: wavelength is λ=633 nm, focal length is f = 633 nm (NA=1), microrelief height is h=0.24 μm, discretization step is 22 nm, grating period is 220 nm, diffraction grating's groove is 110 nm, and step width is 110 nm. According to ellipsometric measurements, the refined refractive index of amorphous silicon equals n=4.35 + i0.486.

A metalens with the relief of Fig. 9 was fabricated using e-beam lithography. A 130-nm amorphous silicon (a-Si) film sputtered on a pyrex glass (n=1.47) was coated with a 320-nm PMMA resist, which was then fixed at 180C. The resist thickness of 320 nm was chosen to be optimal. A 15-nm gold film was sputtered atop to prevent a surface charge from accumulating. The binary mask (Fig. 9) was transferred into the resist surface using a 30-kV electron beam. The specimen was developed in a 3:7 water solution of isopropanol, with the golden layer entirely washed off the PMMA surface.

The mask was transferred from the resist into the aSi via reactive ion etching in gases CHF_3 and SF_6. The resist thickness was chosen to be able to protect the nanostructured microrelief while etching the 130-nm amorphous aSi. The aspect ratio of etch rates of the material and mask was found to be 1:2.5. Figure 10 shows an electronic microscope image of a metalens, with the entire 30-μm metalens shown in Fig. 10*a* and its magnified central fragment - in Fig. 10*b*.

A portion of the metalens was also measured using an atomic force microscope Solver Pro. Figure 11*a* depicts the central fragment of the metalens microrelief, with the characteristic microrelief profile depicted in Fig. 11*b*. The microrelief depth was found to vary from 80 nm to 160 nm, the average depth being 120 nm. The radius of the microscope's probe tip was 10 nm. The microrelief depth was measured within an error of 5%, with the transverse coordinates measured within a 2.5% error. The experimental characterization of the metalens-aided focal spot was conducted using a near-field optical scanning microscope. The experimental optical setup is shown in Fig. 12*a*.

In the experiment, light from a He-Ne laser (wavelength 633 nm and power 50 mW) travelled through a fiber optic system and illuminated the metalens under study, which generated a subwavelength focal spot. The full width of the incident beam was 30 μm. The intensity distribution across the focal spot was measured using a metallized hollow pyramid probe C *with a 100-nm tip hole. Having passed through the tip hole, the light was directed to a 100x objective* O_1*, passed through a spectrometer* S *(Solar TII, Nanofinder 30), and was registered by a CCD-camera (Andor, DV401-BV). The experimentally measured focal length of the metalens was* z *= 0.6 μm. The intensity pattern in the focus measured on an NSOM is presented in Fig. 12*b. *The maximal intensity in the focus was found to be 11 times that of the incident beam. The experimentally measured size of the focal spot was FWHMx=0.55λ and FWHMy=0.49λ. These values are seen to be just 8% different from the theoretically estimated values of FWHMx=0.52λ and FWHMy=0.46λ, obtained with due account for the fabrication errors.*

Up to this point, we have discussed metalenses based on four space-variant subwavelength gratings, which proved to be sufficient to generate radially and azimuthally polarized light fields. It stands to reason that the greater the spatial variations of the gratings, the greater the accuracy of the resulting desired field. Below, we describe the numerical simulation of a metalens with 16 differently oriented grooves of subwavelength gratings. A metalens in Fig. 13 is similar to that in Fig. 9, but has 16, rather than four, sectors. The simulation parameters were as follows: a plane incident wave (λ=633 nm Ex=1, Ey=Ez=0), metalens focal length- f=633 nm, microrelief height- h=0.12 μm, pixel size- 22 nm, gratings period- 220 nm, grating groove- 110 nm (5 pixels), step width- 110 nm (5 pixels). The picture in Fig. 13 is 8μm×8 μm in size, the aSi gratings have n = 4.35 + i0.486, glass substrate has n = 1.5; the FDTD-aided computation was done with a λ/30 step on all three coordinates.

The resulting near-circular focal spot measured FWHMx=0.390λ and FWHMy=0.401λ. With the metalens's subwavelength gratings arranged so as to convert a linearly polarized incident beam into a radially polarized beam, the entire energy of the focal spot was found in the Ez- component.

7. Discussion

Summarizing the said above, we can conclude the following. Due to the difference of the refractive indices and of the absorption of the TE- and TM-polarized waves passing through the subwavelength relief [3], it is possible to create elements that work similarly to classical wave plates [4], [6] and polarizers [67]. Subwavelength gratings that work similarly to the wave plates are investigated for the visible [7], infrared [6] and terahertz [44] range. Their fabrication for small wavelengths is complicated since a large aspect ratio is required for the grating relief, but, nevertheless, the interest in the fabrication of subwavelength gratings does not decay. The requirement of a high aspect ratio can be circumvented if instead of transmission gratings reflective gratings are used [43], [7]. Due to the possibility of a local change of the relief direction, subwavelength gratings allow generation of polarization-inhomogeneous beams, such as cylindrical vector beams [40].

Combining a subwavelength polarizing grating with classical zone plates allows generation of elements that perform simultaneous polarization conversion and, for example, focusing of laser radiation [11].

8. Conclusions

In this review, we have analyzed recent articles concerned with the design of subwavelength diffraction gratings to control the polarization and phase of the incident light. In more detail, the subwavelength gratings operating as wave-plate analogues intended to generate cylindrical vector beams have been discussed. A simple approach to designing metasurface components based on space-variant subwavelength gratings has been proposed. The approach is different from a conventional method based on the Pancharatnam-Berry phase, not requiring the use of the circularly polarized incident light. Particular examples of operating micropolarizers and metalenses have been discussed.

Funding

This work was supported by the Russian Science Foundation [grant 17-19-01186].

References

[1] V. A. Soifer, *Diffractive Nanophotonics*. CRC Press, 2014.

[2] V. V. Kotlyar and O. K. Zalyalov, "Design of diffractive optical elements modulating polarization," *Optik (Stuttg).*, vol. 103, no. 3, pp. 125–130, 1996.

[3] P. Lalanne and D. Lemercier-Lalanne, "On the effective medium theory of subwavelength periodic structures," *J. Mod. Opt.*, vol. 43, no. 10, pp. 2063–2086, Oct. 1996.

[4] Z. Bomzon, V. Kleiner, and E. Hasman, "Pancharatnam–Berry phase in space-variant polarization-state manipulations with subwavelength gratings," *Opt. Lett.*, vol. 26, no. 18, pp. 1424–1426, Sep. 2001.

[5] Z. Bomzon, G. Biener, V. Kleiner, and E. Hasman, "Radially and azimuthally polarized beams generated by space-variant dielectric subwavelength gratings," *Opt. Lett.*, vol. 27, no. 5, pp. 285–287, Mar. 2002.

[6] G. M. Lerman and U. Levy, "Generation of a radially polarized light beam using space-variant subwavelength gratings at 1064 nm," *Opt. Lett.*, vol. 33, no. 23, pp. 2782–2784, Dec. 2008.

[7] S. S. Stafeev, L. O'Faolain, V. V. Kotlyar, and A. G. Nalimov, "Tight focus of light using micropolarizer and microlens," *Appl. Opt.*, vol. 54, no. 14, pp. 4388–4394, 2015.

[8] N. Yu and F. Capasso, "Flat optics with designer metasurfaces," *Nat. Mater.*, vol. 13, no. 2, pp. 139–150, Jan. 2014.

[9] S. Pancharatnam, "Generalized theory of interference, and its applications," *Proc. Indian Acad. Sci. - Sect. A*, vol. 44, no. 5, pp. 247–262, 1956.

[10] M. V Berry, "The Adiabatic Phase and Pancharatnam's Phase for Polarized Light," *J. Mod. Opt.*, vol. 34, no. 11, pp. 1401–1407, Nov. 1987.

[11] V. V. Kotlyar, A. G. Nalimov, S. S. Stafeev, C. Hu, L. O'Faolain, M. V. Kotlyar, D. Gibson, and S. Song, "Thin high numerical aperture metalens," *Opt. Express*, vol. 25, no. 7, pp. 8158–8167, Apr. 2017.

[12] Q. Zhan, "Cylindrical vector beams: from mathematical concepts to applications," *Adv. Opt. Photonics*, vol. 1, no. 1, pp. 1–57, 2009.

[13] R. Dorn, S. Quabis, and G. Leuchs, "Sharper focus for a radially polarized light beam," *Phys. Rev. Lett.*, vol. 91, no. 23, p. 233901, 2003.

[14] Y. I. Salamin, Z. Harman, and C. H. Keitel, "Direct High-Power Laser Acceleration of Ions for Medical Applications," *Phys. Rev. Lett.*, vol. 100, no. 15, p. 155004, Apr. 2008.

[15] X. Hao, C. Kuang, T. Wang, and X. Liu, "Phase encoding for sharper focus of the azimuthally polarized beam.," *Opt. Lett.*, vol. 35, no. 23, pp. 3928–3930, Dec. 2010.

[16] J. F. de Boer and T. E. Milner, "Review of polarization sensitive optical coherence tomography and Stokes vector determination.," *J. Biomed. Opt.*, vol. 7, no. 3, pp. 359–371, 2002.

[17] X. Li, J. W. M. Chon, S. Wu, R. A. Evans, and M. Gu, "Rewritable polarization-encoded multilayer data storage in 2, 5-dimethyl-4-(p-nitrophenylazo) anisole doped polymer," *Opt. Lett.*, vol. 32, no. 3, pp. 277–279, 2007.

[18] M. Noto, D. Keng, I. Teraoka, and S. Arnold, "Detection of Protein Orientation on the Silica Microsphere Surface Using Transverse Electric/Transverse Magnetic Whispering Gallery Modes," *Biophys. J.*, vol. 92, no. 12, pp. 4466–4472, Jun. 2007.

[19] Z. Ghadyani, I. Vartiainen, I. Harder, W. Iff, A. Berger, N. Lindlein, and M. Kuittinen, "Concentric ring metal grating for generating radially polarized light," *Appl. Opt.*, vol. 50, no. 16, pp. 2451–2457, Jun. 2011.

[20] J. Lin, P. Genevet, M. A. Kats, N. Antoniou, and F. Capasso, "Nanostructured holograms for broadband manipulation of vector beams," *Nano Lett.*, vol. 13, no. 9, pp. 4269–4274, 2013.

[21] P. Genevet and F. Capasso, "Holographic optical metasurfaces: a review of current progress.," *Rep. Prog. Phys.*, vol. 78, no. 2, p. 24401, 2015.

[22] B. Päivänranta, N. Passilly, J. Pietarinen, P. Laakkonen, M. Kuittinen, and J. Tervo, "Low-cost fabrication of form-birefringent quarter-wave plates," *Opt. Express*, vol. 16, no. 21, pp. 16334–16342, Oct. 2008.

[23] M.-Y. Lin, T.-H. Tsai, Y. L. Kang, Y.-C. Chen, Y.-H. Huang, Y.-J. Chen, X. Fang, H. Y. Lin, W.-K. Choi, L. A. Wang, C.-C. Wu, and S.-C. Lee, "Design and fabrication of birefringent nano-grating structure for circularly polarized light emission," *Opt. Express*, vol. 22, no. 7, pp. 7388–7398, 2014.

[24] M. Y. Lin, T. H. Tsai, L. J. Hsiao, W. C. Tu, S. H. Wu, L. A. Wang, S. C. Lee, and H. Y. Lin, "Design and Fabrication of Nano-Structure for Three-Dimensional Display Application," *IEEE Photonics Technol. Lett.*, vol. 28, no. 8, pp. 884–886, 2016.

[25] U. Levy, C.-H. Tsai, L. Pang, and Y. Fainman, "Engineering space-variant inhomogeneous media for polarization control," *Opt. Lett.*, vol. 29, no. 15, pp. 1718–1720, Aug. 2004.

[26] G. M. Lerman and U. Levy, "Radial polarization interferometer," *Opt. Express*, vol. 17, no. 25, pp. 23234–23246, Dec. 2009.

[27] T. Kämpfe and O. Parriaux, "Depth-minimized, large period half-wave corrugation for linear to radial and azimuthal polarization transformation by grating-mode phase management.," *J. Opt. Soc. Am. A. Opt. Image Sci. Vis.*, vol. 28, no. 11, pp. 2235–2242, 2011.

[28] T. Kämpfe, P. Sixt, D. Renaud, A. Lagrange, F. Perrin, and O. Parriaux, "Segmented subwavelength silicon gratings manufactured by high productivity microelectronic technologies for linear to radial/azimuthal polarization conversion," *Opt. Eng.*, vol. 53, no. 10, p. 107105, 2014.

[29] S. S. Stafeev, A. G. Nalimov, M. V. Kotlyar, D. Gibson, S. Song, L. O'Faolain, and V. V. Kotlyar, "Microlens-aided focusing of linearly and azimuthally polarized laser light," *Opt. Express*, vol. 24, no. 26, 2016.

[30] S. S. Stafeev, M. V. Kotlyar, L. O'Faolain, A. G. Nalimov, and V. V. Kotlyar, "A four-zone transmission azimuthal micropolarizer with phase shift," *Comput. Opt.*, vol. 40, no. 1, pp. 12–18, Jan. 2016.

[31] K. Debnath, L. O'Faolain, F. Y. Gardes, A. G. Steffan, G. T. Reed, and T. F. Krauss, "Cascaded modulator architecture for WDM applications.," *Opt. Express*, vol. 20, no. 25, pp. 27420–27428, 2012.

[32] T. Paul, A. Matthes, T. Harzendorf, S. Ratzsch, and U. D. Zeitner, "Half-wave phase retarder working in transmission around 630nm realized by atomic layer deposition of sub-wavelength gratings," *Opt. Mater. Express*, vol. 5, no. 1, pp. 124–129, Jan. 2015.

[33] T. Kämpfe, S. Tonchev, G. Gomard, C. Seassal, and O. Parriaux, "Hydrogenated amorphous silicon microstructuring for 0th-order polarization elements at 1.0-1.1 μm wavelength," *IEEE Photonics J.*, vol. 3, no. 6, pp. 1142–1148, 2011.

[34] K. Ventola, J. Tervo, P. Laakkonen, and M. Kuittinen, “High phase retardation by waveguiding in slanted photonic nanostructures,” *Opt. Express*, vol. 19, no. 1, pp. 241–246, Jan. 2011.

[35] I. Yamada, N. Yamashita, T. Einishi, M. Saito, K. Fukumi, and J. Nishii, “Design and fabrication of an achromatic infrared wave plate with Sb–Ge–Sn–S system chalcogenide glass,” *Appl. Opt.*, vol. 52, no. 7, p. 1377, Mar. 2013.

[36] I. Yamada, N. Yamashita, K. Tani, T. Einishi, M. Saito, K. Fukumi, and J. Nishii, “Fabrication of a mid-IR wire-grid polarizer by direct imprinting on chalcogenide glass,” *Opt. Lett.*, vol. 36, no. 19, p. 3882, Oct. 2011.

[37] T. Mori, N. Yamashita, H. Kasa, K. Fukumi, K. Kintaka, and J. Nishii, “Periodic sub-wavelength structures with large phase retardation fabricated by glass nanoimprint,” *J. Ceram. Soc. Japan*, vol. 117, no. 1370, pp. 1134–1137, 2009.

[38] H. Zhao and D. Yuan, “Quarter wave retarder design with subwavelength gratings based on modal method,” *Opt. - Int. J. Light Electron Opt.*, vol. 127, no. 1, pp. 212–214, 2016.

[39] A. G. Nalimov, L. O’Faolain, S. S. Stafeev, M. I. Shanina, and V. V. Kotlyar, “Reflected four-zones subwavelength microoptics element for polarization conversion from linear to radial,” *Comput. Opt.*, vol. 38, no. 2, pp. 229–236, 2014.

[40] V. V. Kotlyar, S. S. Stafeev, M. V. Kotlyar, A. G. Nalimov, and L. O’Faolain, “Subwavelength micropolarizer in a gold film for visible light,” *Appl. Opt.*, vol. 55, no. 19, pp. 5025–5032, Jul. 2016.

[41] S. S. Stafeev, A. G. Nalimov, M. V. Kotlyar, and L. O’Faolain, “A four-zone reflective azimuthal micropolarizer,” *Comput. Opt.*, vol. 39, no. 5, pp. 709–715, Dec. 2015.

[42] I. Yamada, “Fabrication and evaluation of reflective wave plate with subwavelength grating structure,” in *Proceedings of SPIE*, 2016, vol. 9888, p. 98880P.

[43] I. Yamada, T. Ishihara, and J. Yanagisawa, “Reflective waveplate with subwavelength grating structure,” *Jpn. J. Appl. Phys.*, vol. 54, no. 9, p. 92203, 2015.

[44] S. C. Saha, Y. Ma, J. P. Grant, A. Khalid, and D. R. S. Cumming, “Imprinted terahertz artificial dielectric quarter wave plates,” *Opt. Express*, vol. 18, no. 12, pp. 12168–12175, Jun. 2010.

[45] S. C. Saha, Y. Ma, J. P. Grant, A. Khalid, and D. R. S. Cumming, “Imprinted quarter wave plate at terahertz frequency,” *J. Vac. Sci. Technol. B, Nanotechnol. Microelectron. Mater. Process. Meas. Phenom.*, vol. 28, no. 6, p. C6M83-C6M87, Nov. 2010.

[46] S. C. Saha, M. Yong, J. P. Grant, A. Khalid, and D. R. S. Cumming, “Low-loss terahertz artificial dielectric birefringent quarter-wave plates,” *IEEE Photonics Technol. Lett.*, vol. 22, no. 2, pp. 79–81, 2010.

[47] B. Zhang, Y. Gong, and H. Dong, “Thin-form birefringence quarter-wave plate for lower terahertz range based on silicon grating,” *Opt. Eng.*, vol. 52, no. 3, p. 30502, Feb. 2013.

[48] Y. Gong and H. Dong, “Terahertz waveplate made with transparency,” *37th Int. Conf. Infrared, Millimeter, Terahertz Waves, IRMMW-THz*, pp. 1–2, 2012.

[49] Y. Gong, Z. Chen, and M. Hong, “Investigation on Terahertz waveplate at upper Terahertz band,” in *2011 International Conference on Infrared, Millimeter, and Terahertz Waves*, 2011, pp. 1–2.

[50] B. Zhang and Y. Gong, “Achromatic terahertz quarter waveplate based on silicon grating,” *Opt. Express*, vol. 23, no. 10, p. 14897, 2015.

[51] L. Sun, Z. Lü, D. Zhang, Z. Zhao, and J. Yuan, “Achromatic terahertz quarter-wave

retarder in reflection mode," *Appl. Phys. B Lasers Opt.*, vol. 106, no. 2, pp. 393–398, 2012.

[52] V. P. Yakunin, A. V Nesterov, and V. G. Niziev, "Generation of high power radially polarized beam," in *Proceedings of SPIE*, 2000, vol. 3889, pp. 718–724.

[53] Z. Zhang, F. Dong, T. Cheng, K. Qiu, Q. Zhang, W. Chu, and X. Wu, "Nano-fabricated pixelated micropolarizer array for visible imaging polarimetry," *Rev. Sci. Instrum.*, vol. 85, no. 10, p. 105002, 2014.

[54] Y. Yang, W. Wang, P. Moitra, I. I. Kravchenko, D. P. Briggs, and J. Valentine, "Dielectric Meta-Reflectarray for Broadband Linear Polarization Conversion and Optical Vortex Generation," *Nano Lett.*, vol. 14, no. 3, pp. 1394–1399, Mar. 2014.

[55] S. Sun, K. Yang, C. Wang, T. Juan, W. T. Chen, C. Y. Liao, Q. He, S. Xiao, W. Kung, G. Guo, L. Zhou, and D. P. Tsai, "High-Efficiency Broadband Anomalous Reflection by Gradient Meta-Surfaces," *Nano Lett.*, vol. 12, no. 12, pp. 6223–6229, Dec. 2012.

[56] L. Lan, W. Jiang, and Y. Ma, "Three dimensional subwavelength focus by a near-field plate lens," *Appl. Phys. Lett.*, vol. 102, no. 23, p. 231119, Jun. 2013.

[57] L. Verslegers, P. B. Catrysse, Z. Yu, J. S. White, E. S. Barnard, M. L. Brongersma, and S. Fan, "Planar Lenses Based on Nanoscale Slit Arrays in a Metallic Film," *Nano Lett.*, vol. 9, no. 1, pp. 235–238, Jan. 2009.

[58] F. Aieta, P. Genevet, M. A. Kats, N. Yu, R. Blanchard, Z. Gaburro, and F. Capasso, "Aberration-Free Ultrathin Flat Lenses and Axicons at Telecom Wavelengths Based on Plasmonic Metasurfaces," *Nano Lett.*, vol. 12, no. 9, pp. 4932–4936, Sep. 2012.

[59] A. Arbabi, Y. Horie, A. J. Ball, M. Bagheri, and A. Faraon, "Subwavelength-thick lenses with high numerical apertures and large efficiency based on high-contrast transmitarrays," *Nat. Commun.*, vol. 6, no. May, p. 7069, May 2015.

[60] A. Arbabi, Y. Horie, M. Bagheri, and A. Faraon, "Dielectric metasurfaces for complete control of phase and polarization with subwavelength spatial resolution and high transmission," *Nat. Nanotechnol.*, vol. 10, no. 11, pp. 937–943, Aug. 2015.

[61] X. Ni, S. Ishii, A. V Kildishev, and V. M. Shalaev, "Ultra-thin, planar, Babinet-inverted plasmonic metalenses," *Light Sci. Appl.*, vol. 2, no. 4, p. e72, Apr. 2013.

[62] P. R. West, J. L. Stewart, A. V Kildishev, V. M. Shalaev, V. V Shkunov, F. Strohkendl, Y. A. Zakharenkov, R. K. Dodds, and R. Byren, "All-dielectric subwavelength metasurface focusing lens," *Opt. Express*, vol. 22, no. 21, pp. 26212–26221, Oct. 2014.

[63] D. Lin, P. Fan, E. Hasman, and M. L. Brongersma, "Dielectric gradient metasurface optical elements," *Science (80-.).*, vol. 345, no. 6194, pp. 298–302, Jul. 2014.

[64] V. V Kotlyar, S. S. Stafeev, Y. Liu, L. O'Faolain, and A. A. Kovalev, "Analysis of the shape of a subwavelength focal spot for the linearly polarized light," *Appl. Opt.*, vol. 52, no. 3, pp. 330–339, Jan. 2013.

[65] V. V. Kotlyar, A. G. Nalimov, and M. V. Kotlyar, "Modeling a polarization microlens to focus linearly polarized light into a near-circular subwavelength focal spot," *Comput. Opt.*, vol. 40, no. 4, pp. 451–457, Jan. 2016.

[66] S. S. Stafeev, V. V. Kotlyar, and L. O'Faolain, "Subwavelength focusing of laser light by microoptics," *J. Mod. Opt.*, vol. 60, no. 13, pp. 1050–1059, Jul. 2013.

[67] A. V. Nesterov and V. G. Niziev, "Laser beams with axially symmetric polarization," *J. Phys. D. Appl. Phys.*, vol. 33, pp. 1817–1822, 2000.

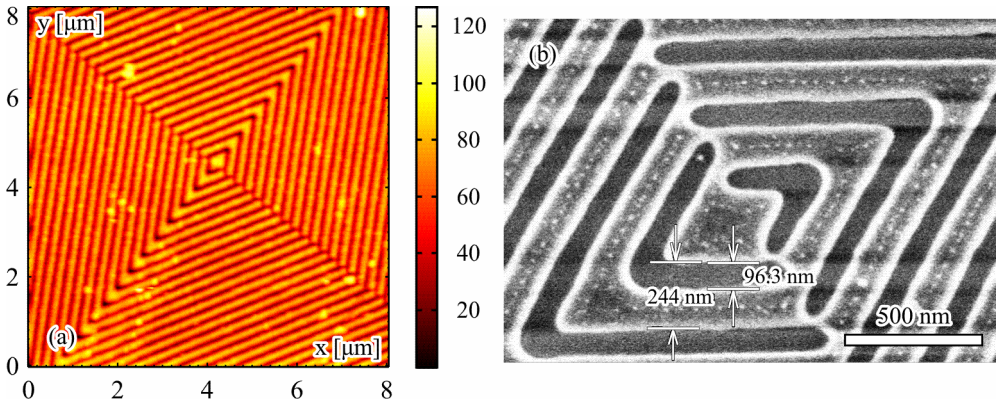

Fig. 1. AFM and SEM images of a micropolarizer in transmission mode [29].

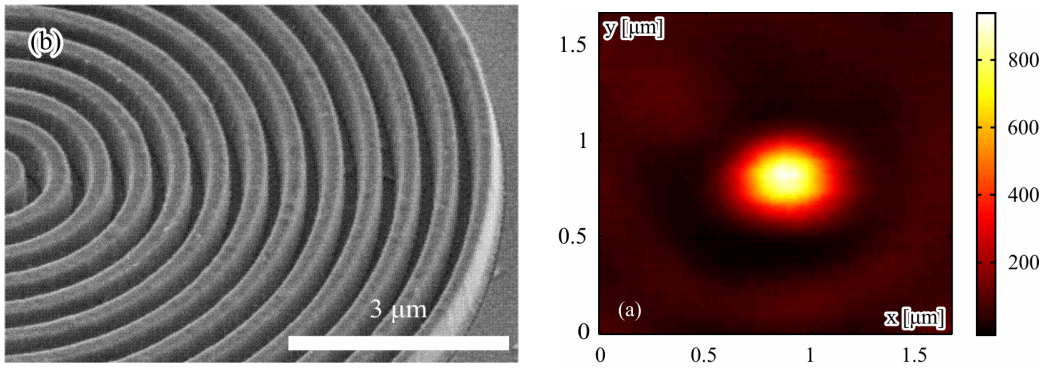

Fig.2 SEM image of ZP (a) and 2D intensity distribution of the focal spot measured using a NSOM Integra Spectra (b) [29]

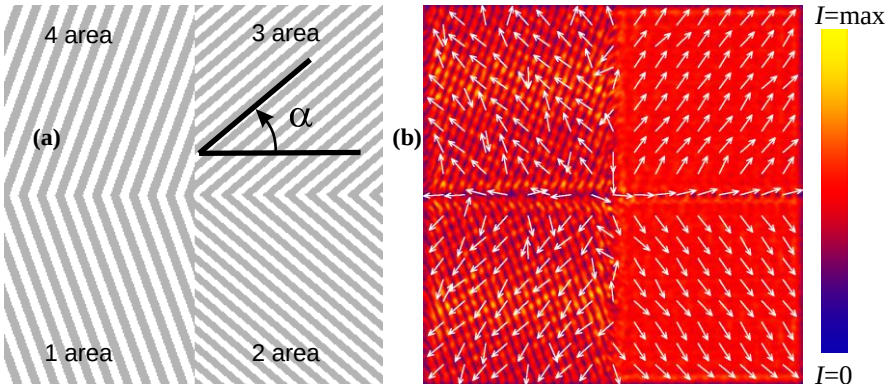

Fig. 3 (a) The layout of a four-sector micropolarizer composed of four subwavelength binary diffraction gratings with period 460 nm (for the incident wavelength of 633 nm) in a gold film and (b) the near-surface intensity distribution of the reflected light. Arrows show the polarization direction in each sector [11].

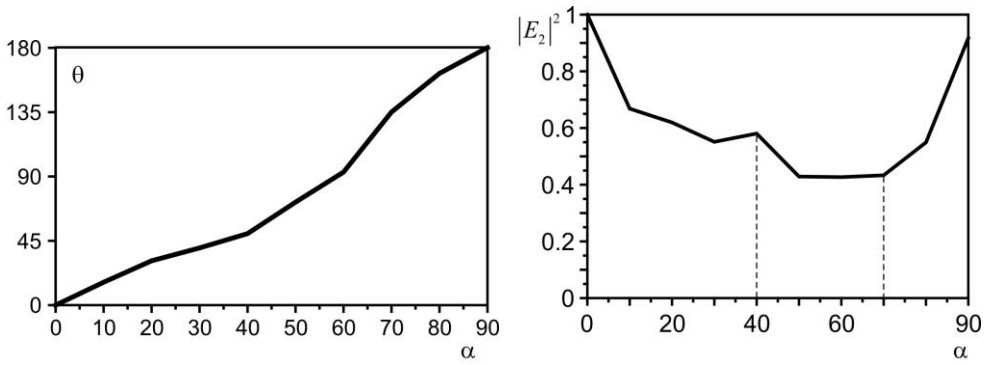

Fig.4 The angles α and θ respectively define a change in the groove tilt and the reflected electric field vector, (a) the angle of the polarization vector θ vs the incident electric vector angle α, and (b) reflected field intensity $|E_2|^2$ *vs. the grating's groove angle α.* [40]

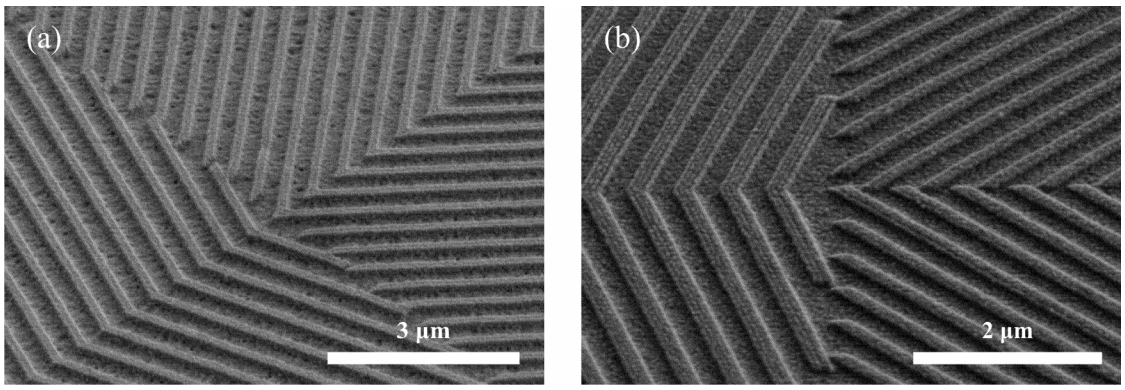

Fig.5 SEM images of micropolarizers for (a) radial [7] *and (b) azimuthal* [40] *polarization.*

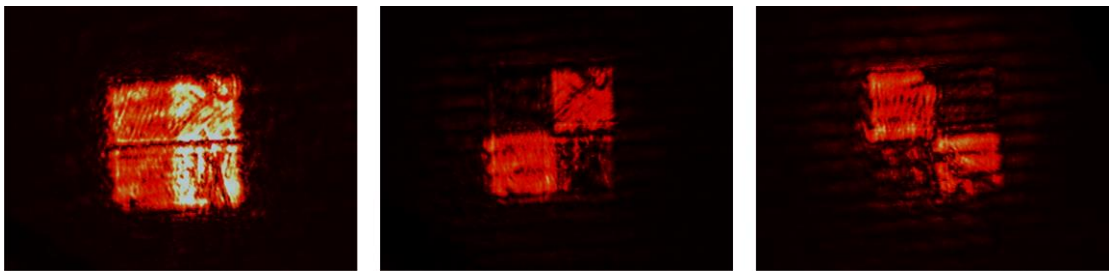

Fig.6 Image of a 100x100-μm four-sector micropolarizer (Fig.5a) obtained in reflection under illumination by a 633-nm laser beam for the differently directed axis of the output polarizer (put before a CCD-camera): 0°(a), 45°(b), -45°(c). [7]

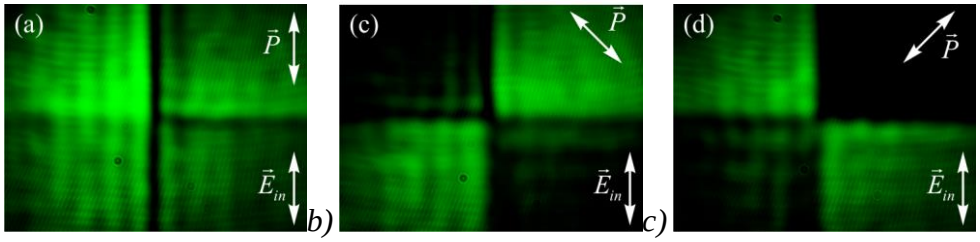

Fig.7 Image of a 100x100-μm four-sector micropolarizer (Fig.5b) obtained in reflection under illumination by a 532-nm laser beam for the differently directed axis of the output polarizer (put before a CCD-camera): 0°(a), -45°(b), 45°(c). The incident light is vertically polarized. [40]

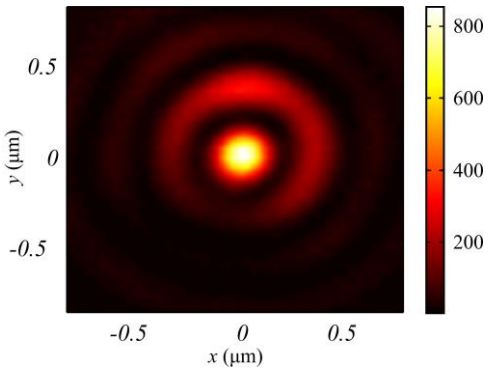

Fig.8 An illustration of a SNOM-aided intensity distribution when a beam reflected at the micropolarizer (Fig.5b) is focused by the microlens (Fig.2a). [7]

Fig. 9 Microrelief pattern of a metalens in transmission to simultaneously perform linear-to radial polarization conversion and focus light. [11]

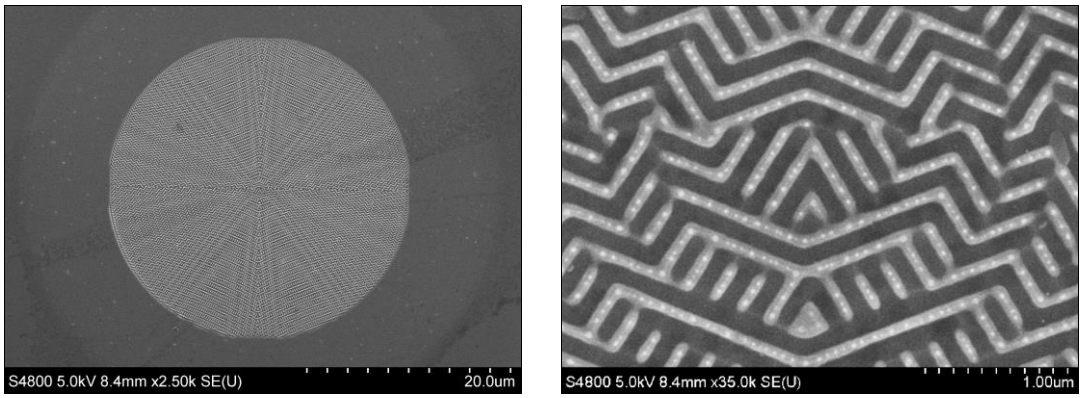

Fig. 10 (a) An electronic microscope image of a 30-μm metalens in an aSi and (b) its magnified 3μm ×2 μm central fragment. [11]

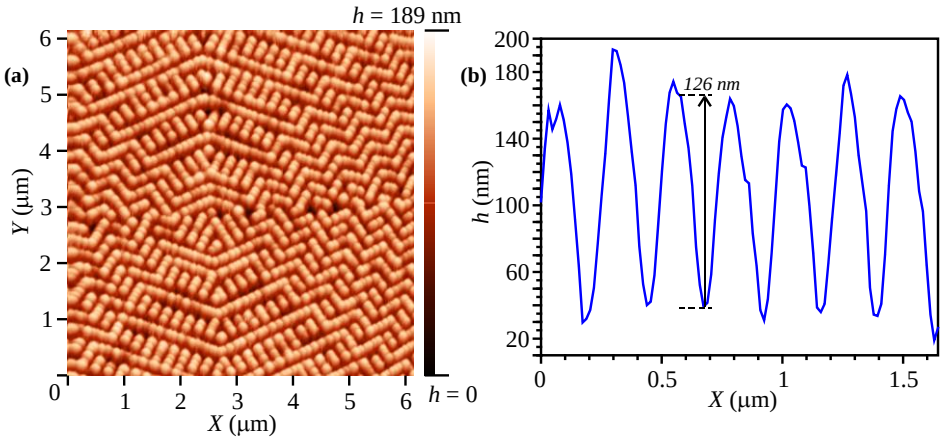

Fig. 11. (a) An atomic-force microscope image of a metalens fragment and (b) microrelief profile of a metalens fragment. [11]

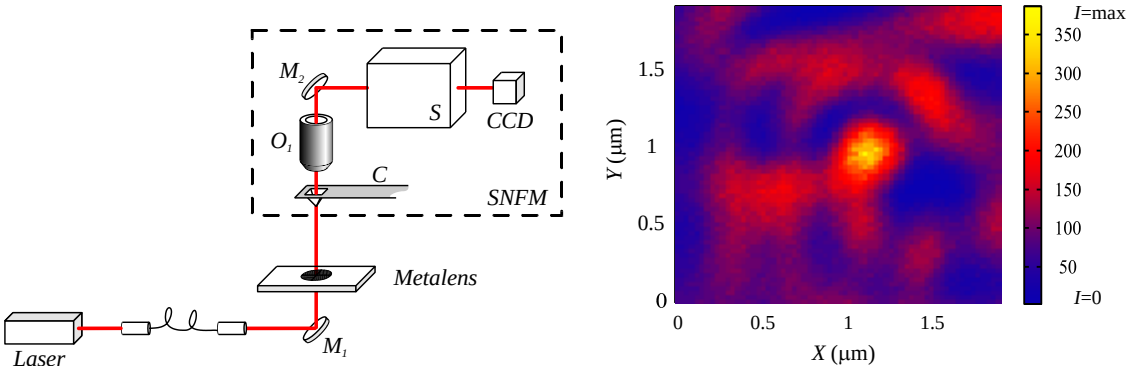

Fig. 12 (a) An experimental optical setup: M_1, M_2- mirrors, O_1 - a 100× objective, C- a probe, S- a spectrometer, and CCD- a CCD-camera. (b) The intensity pattern at distance z=0.6 μm from the metalens. [11]

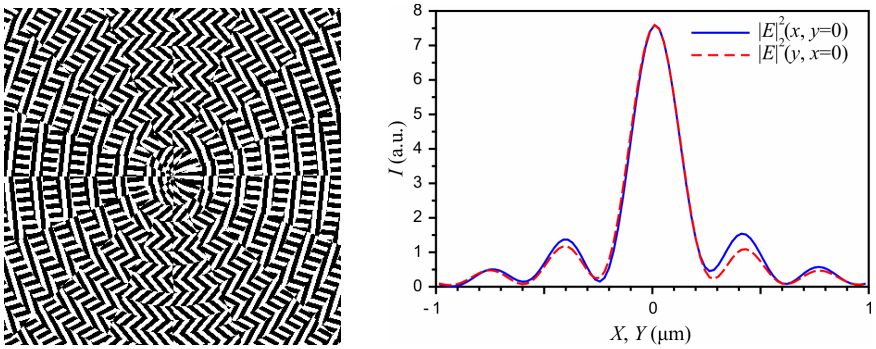

Fig. 13 (a) The binary relief of an aSi metalens whose focus is equal to the incident wavelength, f=λ=633 nm and (b) Intensity profiles drawn via focal spot center along the X- and Y-axes 600-nm away from the metalens surface. [11]